

Nocturnal Eye-Inspired Liquid-to-Gas Phase Change Soft Actuator with Laser-Induced-Graphene : Enhanced Environmental Light Harvesting and Photothermal Conversion

Main Sogabe^{1†}, Youhyun Kim^{1†}, Kenji Kawashima^{1*}

¹Department of Information Physics and Computing,

Graduate School of Information Science and Technology,

The University of Tokyo, Hongo 7-3-1, Bunkyo-ku, Tokyo 113-8656, Japan.

*Corresponding author. Email: kenji.kawashima@ipc.i.u-tokyo.ac.jp

[†]These authors contributed equally to this work.

The mobility of robotic systems is fundamentally constrained by their power sources and wiring requirements. While electrical actuation systems have achieved autonomy through battery power and wireless control, pneumatic actuators remain tethered to air supply sources. Liquid-to-gas phase change actuators utilizing low-boiling-point liquids offer a potential liquid, though they typically require substantial thermal input through heating elements that maintain electrical dependencies. External heat sources, particularly light energy, present an alternative for terrestrial applications. However, silicone-based materials, despite their optical transparency, have high volumetric heat capacity and low thermal conductivity, limiting efficient photothermal energy transfer. Previous attempts to address this through graphene or metallic powder incorporation have compromised material properties, including reduced transparency and altered elastic moduli. Inspired by

the tapetum lucidum structure found in nocturnal animals' eyes for efficient light utilization in low-light conditions, this study proposes a novel anisotropic bilayer soft actuator incorporating Laser-Induced Graphene (LIG) on the inner surface of the light-irradiated silicone layer. This creates an anisotropic structure with enhanced photothermal conversion capabilities while maintaining the advantageous properties of silicone. Comparative analysis demonstrates that the proposed actuator exhibits significantly higher photo-induced bending efficiency compared to conventional silicone-based actuators. The response time (T63) improved by 54%, decreasing from 142 seconds for pure silicone to 65 seconds, with recovery response time showing a 48% improvement. This design maintains silicone's transparency and flexibility while utilizing LIG, which can be fabricated under ambient conditions, facilitating both manufacturing and diverse applications.

1 Introduction

Currently, most robotic actuators rely on electrical energy. For example, although pneumatic actuators use air as the driving source, they rely on electrical energy for control and to supply pressed air (1) (2). Therefore, they cannot be considered completely independent of electrical energy. Throughout history, humans have utilized various forms of energy to enrich their lives. Aiming to use energy sources other than electrical energy to drive soft robots can significantly contribute to diversifying actuation methods in robotics.

Several methods have been proposed on using heating methods, such as laser irradiation (3) (4), microwave (5) , heatsink (6) and electromagnetic (7) (8). Kim et al. developed an electrothermal pneumatic actuator using nanofiber mats, achieving a lightweight soft actuator that can operate without external devices by utilizing liquid evaporation (9). However, this approach faces issues such as high power dependency and slow response times.

Various proposals have been made, starting with actuators like pouch motors ((10))((11))((12))((13))that utilize liquid-to-gas phase change, including pneumatic actuators driven by ambient temperature ((14)). However, these actuators operate relatively slowly, with many functioning at frequencies below 0.1 Hz. This is due to significant losses in converting environmental energy

into driving energy and issues related to heat transfer and thermal conductivity. Sogabe et al. (15) developed a small soft actuator that operates in environments rich in thermal energy, such as warm water. This innovation improved the actuation time for bending to around one second using only environmental energy. However, this actuator leverages the thermal properties of the surrounding water (specific heat capacity of $4186 \text{ J/kg} \cdot \text{K}$ (16)) and is thus limited to underwater use.

To enable use in more diverse environments, systems capable of operating on land are required. A solar-driven actuator presents a promising approach to solving these issues (17). Shao et al. proposed an actuator that absorbs environmental light energy through blackbody radiation by mixing graphite into silicone, converting it into thermal energy, and driving it using the liquid-to-gas phase change (methanol) (18). However, this method results in the loss of actuator transparency due to the use of graphite, and adding powders like graphite reduces the Young's modulus, leading to constraints on the actuator's shape and functionality.

Therefore, developing a mechanism that efficiently absorbs environmental energy, enabling actuation even with highly transparent silicone actuators, is crucial. We introduce mechanisms inspired by biological systems that efficiently absorb environmental energy into the actuator.

Bio-inspiration for efficient use of environmental energy

Nocturnal animals need to hunt and escape predators under the faint light of the moon and stars. To efficiently transmit this minimal light to the retinal photoreceptors, they possess a special structure called the tapetum lucidum (Fig. 1A). This structure captures light that passes through the photoreceptors and reflects it back to the retinal layer, stimulating the photoreceptors once again. Inspired by the relationship between the tapetum and the retina, which 'recovers and reuses' light that would otherwise escape, our study proposes the introduction of a new light-reusing bilayer structure that enables liquid-to-gas phase change, which is inefficient with silicone layers alone.

In this study, we employed to use Laser Induced Graphene (LIG) as the photothermal conversion element for the "tapetum" layer. In recent years, Laser-Induced Graphene (LIG) has emerged as a prominent research focus in the field of direct laser writing techniques, where organic materials such as polyimide are transformed into graphene-like structures. LIG is characterized by the formation of a porous three-dimensional graphene network structure, produced through rapid

thermal carbonization (pyrolysis) via laser irradiation. Lin et al. proposed a method to directly graphenize polyimide film surfaces using CO₂ laser irradiation (19). Subsequently, Chyan et al. (20) demonstrated the versatility of LIG fabrication on diverse substrates including textiles, paper, and food products through repeated laser exposure, thereby accelerating its application in flexible devices. LIG has garnered significant attention as a photothermal conversion material that requires no electrical connections or external wiring. It exhibits efficient light-to-heat conversion properties under laser or lamp irradiation and demonstrates transferability to elastomeric substrates. For instance, Dallinger et al. developed an actuator by transferring LIG onto PDMS-based hydrogel sheets, where the generated heat induced humidity changes in the sheet, resulting in strain-induced bending (21). These characteristics have positioned LIG as a promising material for applications in bioelectronics and soft actuators (22).

Building upon these advances, we focused on expanding LIG's applications to liquid-to-gas phase change actuators. We added a LIG layer to conventional silicone soft actuators (15) to enable efficient light-driven actuation. We propose a novel anisotropic bilayer structure where a LIG layer is positioned on the light-incident surface inside highly transparent silicone. This design, inspired by the eyes of nocturnal animals, enables efficient light collection and photothermal conversion. The converted thermal energy is transferred to the internal fluid, causing deformation of the silicone actuator and resulting in controlled bending motion. In this study, we present the fabrication process of the proposed actuator and evaluate its performance characteristics. Furthermore, to demonstrate the practical applicability of our system, we developed a multi-finger robot where multiple units of these novel actuators operate synchronously in response to light stimuli.

2 Concept and fabrication process

2.1 Concept

Figure 1 illustrates the conceptual design of our proposed actuator. While previous phase-change actuators typically employed homogeneous structures, our novel approach focuses on the layered wall architecture to achieve efficient light absorption. As previously discussed, biological eyes utilize a structure called the tapetum to reflect escaped light, thereby increasing photoreceptor

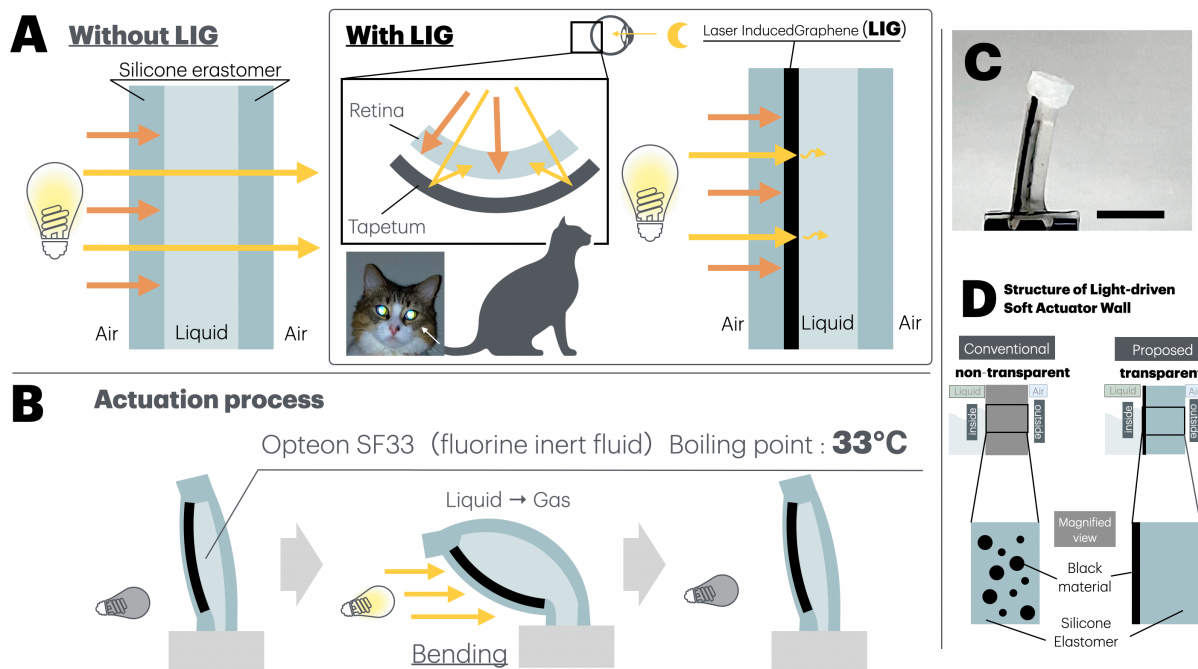


Figure 1: Concept and background of the proposed actuator. A: Structure of tapetum lucidum in nocturnal animals' eyes and its application to the proposed actuator concept utilizing enhanced light absorption efficiency and photothermal conversion as driving force. Inset shows an actual photograph of feline tapetum lucidum (white arrow). B: Schematic illustration of the actuator's driving mechanism and operational principles. C: Photograph of the fabricated actuator prototype. Scale bar = 10 mm. D: Comparative analysis between conventional soft actuators utilizing black materials (e.g., graphene) for photothermal conversion and the proposed actuator design, highlighting key differences.

stimulation. Similarly, our design incorporates a Laser-induced graphene (LIG) layer to capture light not absorbed by the conventional silicone elastomer layer, converting it to thermal energy through photothermal conversion to efficiently vaporize and expand the internal low-boiling-point liquid (Fig. 1A).

The actuation mechanism of the proposed device is depicted in Fig. 1B. The soft actuator deforms through the vaporization of an internal low-boiling-point liquid, controlled by an external light source. The actuator is designed with asymmetric silicone wall thicknesses, with the thinner wall on the graphene layer side to induce directional bending toward the LIG layer. The operating temperature was set at 33°C , above room temperature (25°C), and we selected an inert fluorinated

liquid (Opteon SF33, Chemours Company, base compound structure: Cis – $\text{CF}_3\text{CH} = \text{CHCF}_3$) as the working fluid.

Figure 1C shows a photograph of the fabricated actuator. The actuator has an overall length of 20 mm with a flattened elliptical cross-section measuring approximately 5 mm along the major axis and 4 mm along the minor axis. As illustrated in Fig. 1D, our proposed actuator achieves a layered structure using LIG without incorporating thermally conductive materials or photothermal converters directly into the silicone walls. This approach not only facilitates efficient heat transfer but also maintains the transparency of the silicone elastomer, enabling broader applications of the elastomer-based system.

2.2 Examination of LIG layer characteristics

2.2.1 LIG Transfer Process onto Silicone

The LIG patterns are generated on Kapton tape (3 M Polyimide Film Tape 5413, 3 M Company, Minnesota, USA) adhered to a slide glass. The polyimide base of the Kapton tape enables LIG formation through laser irradiation. We utilize a laser system (xTool F1, Makeblock Co., Ltd., Guangdong, China) with specific parameters (200 mm/s speed, 40% power, unidirectional) for LIG patterning.

The LIG sheet was transferred onto silicone (Ecoflex 00-45 Near Clear, Smooth-On, Inc., Pennsylvania, USA). For the transfer process, the LIG sheet, which remained adhered to the slide glass on one side, was positioned and surrounded by a mold. The degassed uncured silicone was then poured into the mold using a vacuum degassing chamber. The curing process was carried out at 60°C for 60 minutes. After curing, the mold was separated from the slide glass and the cured silicone was peeled off the Kapton tape, resulting in the successful transfer of the LIG onto the silicone surface, yielding a silicone substrate with an integrated LIG layer.

2.3 LIG-transferred soft actuator fabrication process

Figure 2 illustrates the fabrication process of a soft actuator with the LIG layer positioned adjacent to the liquid interface. The fabrication process consists primarily of five steps, designated as (i)–(v). Initially, a LIG pattern (2.6 mm × 40 mm) is created using the aforementioned laser parameters.

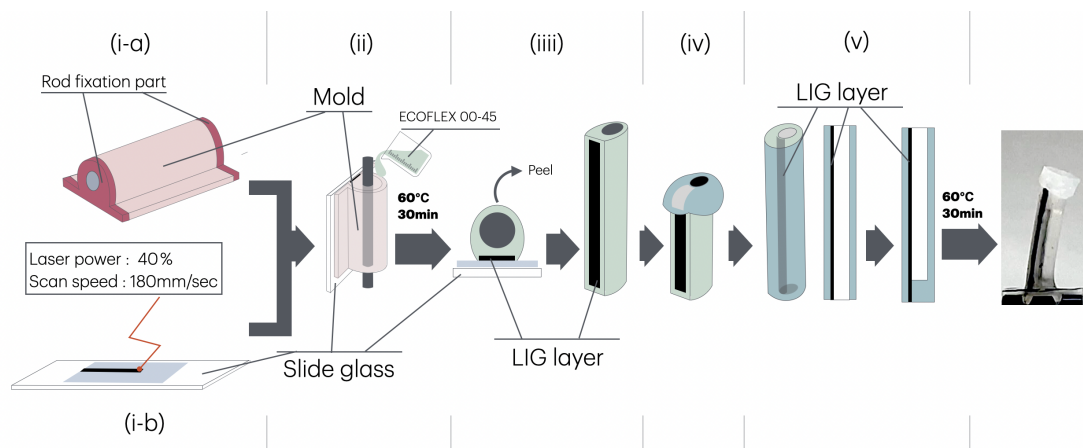


Figure 2: Fabrication process of the proposed actuator. In step (i), a laser-processed plate with LIG printing on slide glass is integrated with a mold component designed to form the tubular structure. Subsequently, in step (ii), a metallic rod (2.5 mm in diameter) is inserted and secured at the rod fixation port, followed by the injection of degassed Ecoflex 00-45. After curing at 60°C for 60 minutes, step (iii) involves carefully removing the mold and peeling the silicone tube from the plate. At this stage, the LIG layer is positioned on the exterior surface; therefore, in step (iv), the tube is inverted. The fabrication process concludes with step (v), where one end of the open-ended tube is sealed with uncured silicone. The actuator becomes operational upon encapsulation with Opteon SF33 and securing the open end with a silicone-coated clip.

The pattern is then positioned and secured within the mold (detailed in Supplementary Data S1) as shown in (i-a). Subsequently, a metallic rod (2.5 mm in diameter) is inserted into the mold, and silicone is introduced and cured as depicted in (ii). In step (iii), the tubular silicone structure with the integrated LIG layer is carefully removed from the mold. Because the LIG layer is initially present on the external surface, the tube is inverted in step (iv) to position the LIG layer on the interior. In step (v), uncured silicone is introduced into one end of the tube to create a seal, resulting in an actuator with one open terminus. The actuator is completed by introducing 40 μ L of a low-boiling-point liquid (Opteon SF33, The Chemours Company, Delaware, USA) into the internal cavity and sealing the open end with a silicone-coated clip.

Additionally, the silicone sheets (10 mm square with transferred LIG patterns) were fabricated using the same process with molds adjusted to achieve a thickness of 1.0 mm. These molds were fabricated using a Formlabs Form 3 printer (Formlabs Inc., Somerville, MA, USA). Clear Resin

v4 (Formlabs Inc.) was utilized as the resin material for mold production.

To investigate whether placing the silicone layer on the exterior and the LIG layer on the interior would affect LIG's photothermal conversion efficiency, we examined the temperature response characteristics. A reflector lamp (RF100 V54 WD, 100 V, 54 W; Panasonic Corporation, Osaka, Japan) was used as the light source, and temperature changes on the silicone sheet were measured using a thermal camera (OPTPI64 ILTO15 T090, Optris GmbH, Berlin, Germany).

Our findings revealed that positioning LIG on the interior actually accelerated the temperature rise at the liquid-contact interface (Supplementary Fig. 1). The initial temperature change rate during the first 5 seconds after light irradiation was 0.71 K/s when irradiated from the silicone side, compared to 0.66 K/s when irradiated from the LIG side (reference value: approximately 0.13 K/s for silicone-only sheet). This phenomenon can be attributed to silicone's high volumetric heat capacity and low thermal conductivity, which impede the efficient transfer of heat generated by LIG to the liquid-contact interface.

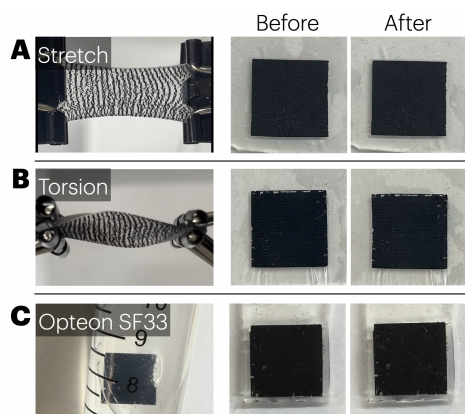


Figure 3: Durability assessment of LIG-transferred silicone under various mechanical and chemical stresses. (A) Resistance to repetitive stretching deformation, (B) resistance to abrasive wear, and (C) resistance to liquid exposure. No delamination or degradation of LIG was observed in any of the test conditions. Scale bar = 10 mm.

2.4 Mechanical and chemical durability of LIG-transferred silicone

Figure 3 illustrates the silicone sheet (10 mm × 10 mm) with a transferred LIG layer, as well as the condition of the LIG after being subjected to 20 cycles of stretching and relaxation, and twisting,

respectively. In both cases, no delamination of the LIG layer was observed.

The resistance of the actuator to the liquid was evaluated by immersing the LIG-transferred sheet into a conical tube filled with Opteon SF33. The actuator was agitated for 60 seconds. After the process, the sheet was examined and no detachment or degradation of the LIG layer was observed, confirming its stability under these conditions (Fig. 4).

3 Heat transfer analysis

When an object is heated by radiation from a heat source at temperature θ_h , the radiative heat transfer Q_{hs} to the silicone wall can be expressed as

$$Q_{hs} = \frac{\sigma(\theta_h^4 - \theta_s^4) A}{\frac{1}{\epsilon_h} + \frac{1}{\epsilon_s} - 1}. \quad (1)$$

Here, $\sigma = 5.67037442 \times 10^{-8} \text{ W} \cdot \text{m}^{-2} \cdot \text{K}^{-4}$ is the Stefan-Boltzmann constant; θ_s is the temperature of the silicone wall; A is the heat transfer area; and ϵ_h and ϵ_s are the emissivities of the heat source and the silicone wall, respectively ((23)). The thermal conductivity of the silicone, λ_s , and its thickness, x , are given in Table 1 (24).

The actuator's response time is sufficiently long. Therefore, the thermal Fourier number becomes large ($F_o \gg 1$) and the temperature distribution within the silicone wall is negligible. The energy balance equation for the silicone wall can then be written as

$$C_s W_s \frac{d\theta_s}{dt} = Q_{hs} - Q_{se} = Q_{hs} - 2 h_{se} A (\theta_s - \theta_e), \quad (2)$$

where C_s is the specific heat capacity of the silicone, W_s is its mass ($W_s = \rho_s A x$), h_{se} is the heat transfer coefficient between the silicone wall and the environment, and θ_e is the environmental temperature (25°C).

Using a difference method, the following equation is derived from Eqs. (1) and (2):

$$\theta_s(t + \Delta t) = \theta_s(t) + \frac{\sigma [\theta_h^4 - \theta_s(t)^4] A}{C_s \rho_s A x \left(\frac{1}{\epsilon_h} + \frac{1}{\epsilon_s} - 1 \right)} - \frac{2 h_{se} [\theta_s(t) - \theta_e]}{C_s \rho_s x}. \quad (3)$$

When the LIG layer is deposited on the side of the silicone wall opposite the heat source, the

heat transfer from the heat source to the LIG layer is

$$Q_{hL} = \frac{\sigma (\theta_h^4 - \theta_L^4) A}{\frac{1}{\epsilon_h} + \frac{1}{\epsilon_L} - 1}, \quad (4)$$

where θ_L is the temperature of the LIG layer and ϵ_L is its emissivity. The energy balance equation for the LIG layer is

$$C_L W_L \frac{d\theta_L}{dt} = Q_{hL} - h_{Le} A (\theta_L - \theta_e) - Q_{Ls}, \quad (5)$$

with

$$Q_{Ls} \simeq \lambda_s A \frac{\theta_L - \theta_s}{x}. \quad (6)$$

Here, C_L is the specific heat capacity of the LIG layer, $W_L = \rho_L A x_L$ is its mass, h_{Le} is the heat transfer coefficient between the LIG layer and the environment, and λ_s is the thermal conductivity of the silicone. Under these conditions, the energy equation of the silicone wall is written as

$$C_s W_s \frac{d\theta_s}{dt} = Q_{hs} - h_{se} A (\theta_s - \theta_e) + Q_{Ls}. \quad (7)$$

The temperature of the LIG layer, $\theta_L(t)$, can be computed by a difference method based on Eqs. (4)–(7).

The parameters used in the simulation are summarized in Table 1 (25). (26)

In this simulation, for the purpose of model simplification, several factors such as Opteon SF33 vaporization and silicone elastomer elongation were not taken into account. The numerical values used for verification were obtained from the referenced literature. Additionally, while the radiative heat transfer equations are presented above, in our actual simulation we simplified the heat transfer calculation by considering the heat source as a light source with constant energy Q_h . The energy absorbed by each material was then calculated using material-specific absorption coefficients (α_s and α_L) which are determined experimentally, where $\alpha_s Q_h$ represents the energy absorbed by the silicone wall and $\alpha_L Q_h$ represents the energy absorbed by the LIG layer.

For comparison with simulation results, we measured the temperature at the liquid contact surface using a thermal camera with silicone sheets of the same thickness as in the simulation (The experimental setup for thermal data acquisition is shown in Fig. 4A, while the corresponding thermal imaging results are presented in Fig. 4B). The results are shown in Fig. 4C. When

Table 1: Parameters used in the simulation

Parameter	Value
$\theta_s(0), \theta_L(0), \theta_e$	298 K
h_{se}	6 W/m ² · K
h_{Le}	25 W/m ² · K
C_s	1300 J/kg · K
C_L	700 J/kg · K
ρ_s	1050 kg/m ³ (27)
ρ_L	400 kg/m ³
λ_s	0.2 W/m · K
α_s	0.17
α_L	0.83
Q_h	0.1 W

overlaying the temporal temperature variations with the simulation graphs, despite some discrepancies, the T63 values showed close agreement: for the case without LIG, the simulation yielded 118.1 seconds while the experimental measurement was 110.7 seconds; for the case with LIG, the simulation predicted 53.9 seconds compared to the experimental value of 58.3 seconds. These results demonstrate that LIG effectively functions as a photothermal conversion and facilitates heat transfer to the internal liquid.

4 Evaluation of a soft actuator with transferred LIG under general light source

4.1 Experimental analysis of actuation driven by light On-Off cycling

The experimental setup is illustrated in Fig. 5. The fabricated actuator was positioned 50 mm away from the light source during the experiments. The light bulb specifications include Central luminance is 300 cd, total luminous flux is 630 lm, and beam angle is 60°. An iPhone 15 Pro

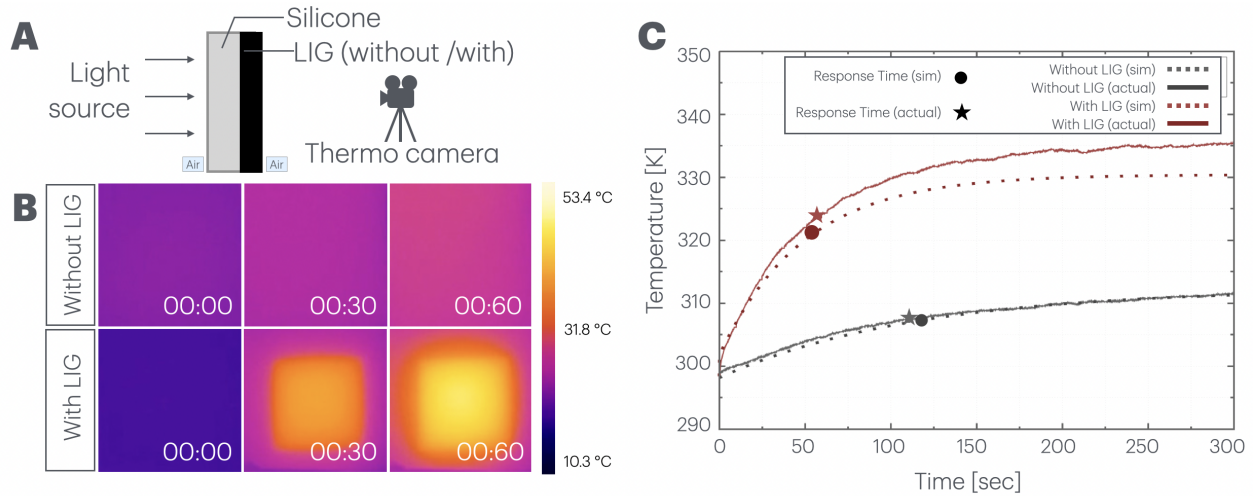


Figure 4: Thermodynamic analysis of temperature changes at liquid-solid interface through thermal imaging and simulation A: Experimental setup for thermal imaging analysis. The measurement was conducted with the distance between the light source and the silicone sheet set to 100 mm. B: Real-time thermal imaging of temperature elevation at the liquid-solid interface comparing silicone sheets with- and without-LIG. The LIG-transferred silicone sheet demonstrated more rapid temperature elevation and higher maximum temperature (334.9 K with-LIG vs. 311.5 K without-LIG). C: Comparison between experimental thermal imaging data (solid lines) and thermodynamic simulation results (dashed lines). Time constant (T63) analysis revealed simulated T63 values of 118.1 sec and 53.9 sec for without- and with-LIG groups, respectively, while experimental measurements yielded T63 values of 110.7 sec and 58.3 sec, respectively.

Max (Apple Inc., Cupertino, CA, USA) was used to capture the actuator deformation, and ImageJ (citation) was employed for analyzing the bending angles and deformation measurements.

Figure 6A and C shows the bending behavior during light irradiation and the subsequent recovery upon light off, along with the corresponding analysis results. When exposed to light, the without-LIG actuator exhibited delayed activation, with a 63% response time of 141.7 seconds and approximately 220 seconds required to reach maximum bending angle. In contrast, the proposed actuator with LIG demonstrated a mean 63% response time of 65.0 seconds and reached maximum bending angle in approximately 90 seconds, showing an 54.1% improvement in responsiveness compared to the without-LIG actuator.

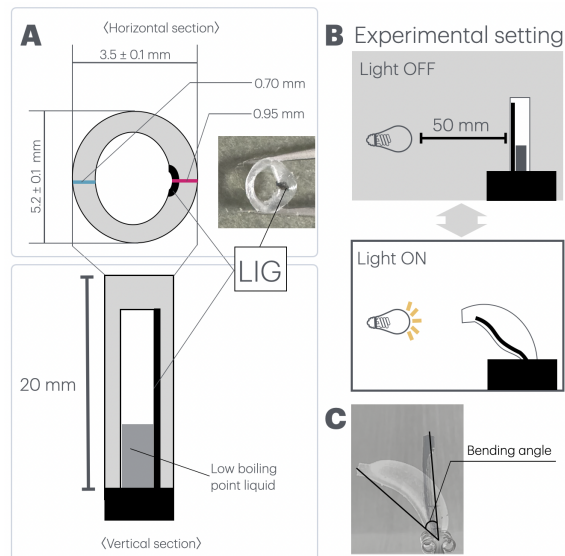


Figure 5: Overview of the proposed actuator and experimental setup. A: Schematic illustration and dimensions of the proposed actuator. The cross-sectional view reveals a distorted elliptical shape, with slight deformation observed at the adhesion interface with the LIG. B: Schematic diagram of the light irradiation experimental setup. The fundamental experiments were conducted with the actuator positioned at a distance of 50 mm from the light source. A 54 W reflector bulb operating at 100 V served as the light source. C: Measurement method of bending angle: The initial state of the actuator before bending was defined as 0 degrees, and the angle by which the tip of the actuator tilted from this position was recorded as the bending angle.

Regarding the recovery phase after light off (Fig 6B and D, the without-LIG actuator showed a 63% response time of 42.7 seconds and required 120 seconds to return to its initial state. The proposed actuator with LIG demonstrated enhanced recovery characteristics with a 63% response time of 22.1 seconds and approximately 60 seconds to return to its initial state, representing an 48.2% improvement in recovery performance compared to the without-LIG actuator.

4.2 Deformation of the actuator before and after light-driven operation

Figure 7 demonstrates the variations in actuator performance based on changes in the encapsulated liquid volume and the distance between the light source and actuator. With the light source fixed at 50 mm, we examined the effect of varying volumes (20 μL , 30 μL , and 40 μL) of encapsulated

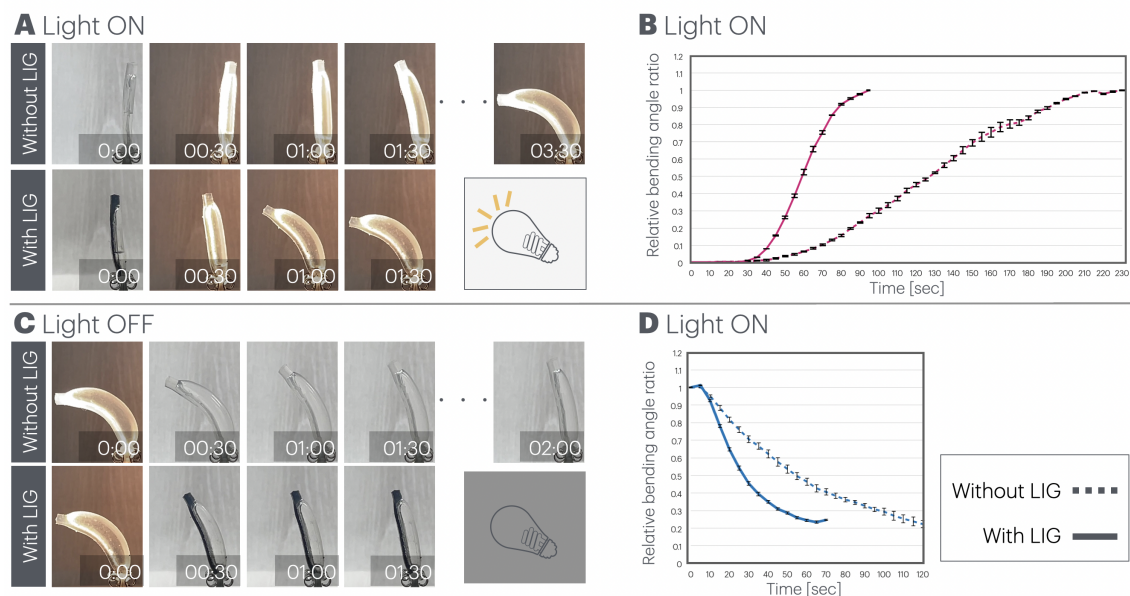


Figure 6: Temporal analysis of bending actuator dynamics. A: Time-lapse photographs illustrating bending deformation during light irradiation with and without LIG. B: Graph of the relative bending angle ratio during light irradiation (n=5). C: Time-lapse photographs depicting the bending recovery process following light deactivation, and D: Corresponding graphical analysis of the relative bending angle ratio changes (n=5). The relative bending angle ratio is defined as the relative angle when the actuator response reaches a plateau (defined as an increase of less than 1 degree over a 20-second proximity period) or the angle in the frame immediately preceding angle reduction, with this value normalized to 1.

Opteon SF33. The results showed volume-dependent increases in three parameters: the rate of actuator deformation (Fig. 7A), the plateau bending angle (Fig. 7B), and the time required to reach the plateau state (Fig. 7C). The linear regression analysis yielded an R^2 value of approximately 0.98, indicating that the relationship can be effectively approximated as linear within the 20-40 μL range.

The influence of external environmental conditions was investigated by varying the distance between the light source and the actuator (50 mm, 75 mm, and 10 mm), with results presented in Fig. 7D-F (Opteon SF33's amount is 30 μL). The deformation ratio and plateau bending angle decreased as the distance increased. Notably, the time required to reach the plateau state was longest in the 100 mm group, showing more than a 2.5-fold increase compared to the 50 mm group.

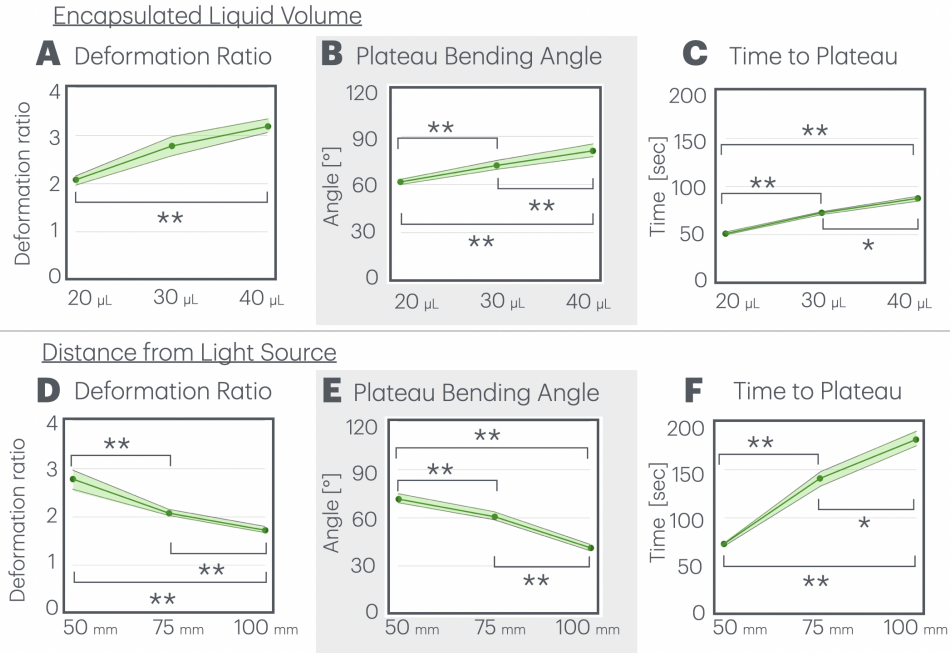


Figure 7: Analysis of LIG-transferred soft actuators under different internal and environmental conditions: A-C: When the distance from the light source was constant (50 mm), the deformation ratio (A), plateau angle (B), and time to reach plateau state (C) were measured for internal liquid volumes of 20, 30, and 40 μL . D-F: When the internal liquid volume was constant (30 μL), the deformation ratio (D), plateau angle (E), and time to reach plateau state (F) were measured for distances of 50, 75, and 100 mm between the light source and actuator. The plateau state was defined as the condition where the angular variation did not increase by more than 1° over a 30-second period. The verification was conducted using three actuators ($n=3$) that exhibited similar plateau angles when operated with an internal volume of 20 μL at a distance of 50 mm from the light source.

5 Multi-Finger Robot Using Non-Contact & Light-Driven LIG-Transferred Soft Actuators

To verify the synchronous actuation capability of multiple LIG-transferred soft actuators, we developed a three-fingered robot inspired by the Venus flytrap and evaluated its operation in ambient conditions. The demonstration is shown in Movie S2 and Fig. 8. As illustrated in Fig. 8, upon irradiation from a light source (a lamp in this experiment), the actuators began to bend

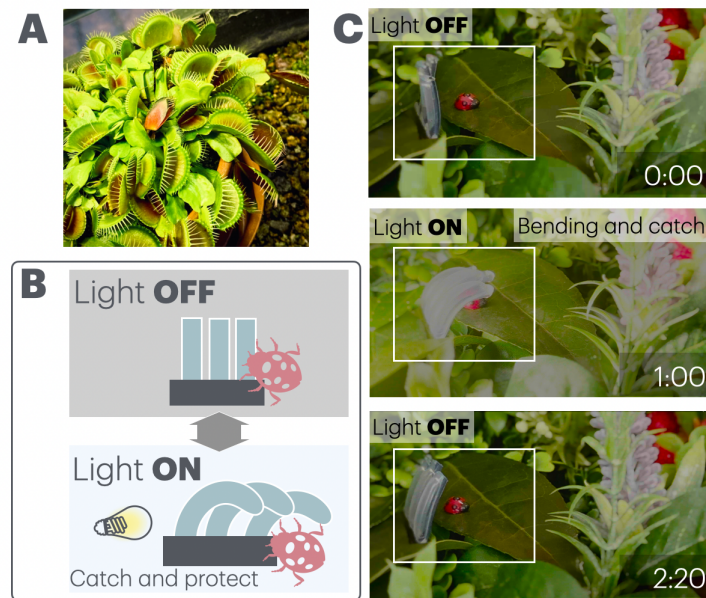


Figure 8: Demonstration of a bio-inspired robot utilizing the proposed actuator in a biomimetic movement driven by light. A: Venus flytrap used as the biomimetic target. B: Conceptual demonstration of the movement, where the robot curves to enclose and retain an object beneath it under light irradiation, and releases it when the light is turning off. C: Actual operation of the robot in the environment, using the same light source as in the experiments. Upon light exposure, the robot captures a miniature ladybug model, protecting and holding it from the light. When irradiation ceases, the robot releases its curvature and frees the enclosed object.

synchronously, successfully enveloping a ladybug-inspired target object through their coordinated curving motion. When the light source was switched off, each actuator released from its bent state and returned to its original configuration.

6 Limitations & future work

6.1 The operating temperature range control

For the actuator’s internal fluid, we employed Opteon SF33 with a boiling point of 33°C. We hypothesize that the operating temperature range can be controlled by varying the boiling point of the encapsulated liquid. For instance, Opteon SF79 and Opteon SF70 have boiling points of 48°C

and 71°C, respectively. Thermal imaging data (Fig. 4B) demonstrates that temperatures approaching 55°C can be achieved when LIG is transferred, suggesting that for terrestrial applications, this system could be implemented with liquids having boiling points in the range of 30-55°C. However, for operations requiring higher temperature ranges, conventional light sources may prove insufficient. In such cases, the implementation of focusing lenses, high-powered lighting systems, or higher-output lasers is required.

6.2 Gas leakage

As shown in Fig. 7F, increasing the distance from the light source resulted in a decrease in the bending angle at plateau. This suggests that Opteon SF33 is leaking out due to silicone's high gas permeability during the slower actuation caused by reduced light intensity. Similar gas leakage phenomena have been discussed in previous studies (15). The current actuator design implements a reusable mechanism where one side is sealed with a clip, allowing multiple refilling of the liquid. However, frequent leakage can limit potential applications. To address this limitation, potential approaches include the incorporation of materials with lower gas permeability and the development of alternative sealing mechanisms.

6.3 Utilization of ambient environmental light

The light source utilized in this study was a reflector lamp (54W) with a beam angle of 60°, center luminous flux of 630 lm, and beam flux of 160 lm. Assuming uniform light distribution, calculations based on illuminance indicate that the actuator surface, positioned at a distance of 50 mm, receives approximately 60,000 lux (assuming an actuator LIG surface area of 40 mm²). This illuminance corresponds to approximately 60% of direct summer sunlight (28). While outdoor operation would be dependent on seasonal and geographical factors, the implementation of lens-based light concentration mechanisms could make outdoor applications feasible. Given that typical office environments maintain illuminance levels of approximately 300–1000 lux (29), indoor operation under ambient lighting conditions would be significantly limited. Future investigations will explore localized light energy irradiation using laser sources, aimed at achieving more precise actuator control at a microscale level.

7 Conclusions

In this paper, we focused on the ocular structure of nocturnal animals that efficiently collect and utilize light in low-irradiation environments. We addressed the limitation of conventional silicone-based soft actuators, which exhibited low driving efficiency due to ineffective light utilization, by incorporating a light-heat conversion element layer called LIG on the light-incident surface. This modification enabled the actuator to effectively utilize light that would otherwise be poorly absorbed by silicone alone, thereby heating the internal low-boiling-point liquid. As a result, the proposed actuator with LIG demonstrated a 54% improvement in response time compared to conventional without-LIG actuators.

While various approaches have successfully enhanced photothermal conversion and thermal conductivity through the incorporation of graphene or metal powders into silicone elastomers, our method explores an alternative approach by installing a LIG layer on the silicone surface. This approach preserves the inherent properties of silicone while utilizing LIG, which can be manufactured under standard environmental conditions, thereby facilitating both the production of photothermal actuators and their diverse applications.

Future research will focus on the versatility of LIG transfer patterns, aiming to develop efficient light-utilizing LIG patterns under natural environmental conditions and design more complex actuator geometries with corresponding LIG patterns. This direction of research aligns with the principles of soft robotics, pursuing the development of soft actuators with enhanced deformation capabilities and environmental adaptability.

References and Notes

1. C. Tawk, G. Alic, A Review of 3D-Printable Soft Pneumatic Actuators and Sensors: Research Challenges and Opportunities. *Advanced Intelligent Systems* **3**, 2000223 (2021), doi:10.1002/aisy.202000223.
2. M. S. Xavier, *et al.*, Soft Pneumatic Actuators: A Review of Design, Fabrication, Modeling, Sensing, Control and Applications. *IEEE Access* **10**, 59442–59485 (2022), doi:10.1109/ACCESS.2022.3179271.
3. F. Meder, G. A. Naselli, A. Sadeghi, B. Mazzolai, Remotely Light-Powered Soft Fluidic Actuators Based on Plasmonic-Driven Phase Transitions in Elastic Constraint. *Advanced Materials* **31**, 1905671. (2019), doi:10.1002/adma.201905671.
4. T. Hiraki, *et al.*, Laser Pouch Motors: Selective and Wireless Activation of Soft Actuators by Laser-Powered Liquid-to-Gas Phase Change. *IEEE Robotics and Automation Letters* **5** (3), 4180–4187 (2020), doi:10.1109/LRA.2020.2982864.
5. S. Ueno, Y. Monnai, Wireless soft actuator based on liquid-gas phase transition controlled by millimeter-wave irradiation. *IEEE Robotics and Automation Letters* **5** (4), 6483–6488 (2020), doi:10.1109/LRA.2020.3013847.
6. Y. Yoon, *et al.*, Bioinspired untethered soft robot with pumpless phase change soft actuators by bidirectional thermoelectrics. *Chemical Engineering Journal* **451**, 138794 (2023), doi:10.1016/j.cej.2022.138794.
7. Y. Tang, *et al.*, Wireless miniature magnetic phase-change soft actuators. *Advanced Materials* **34**, 2204185. (2022), doi:10.1002/adma.202204185.
8. S. M. Mirvakili, D. Sim, I. W. Hunter, R. Langer, Actuation of untethered pneumatic artificial muscles and soft robots using magnetically induced liquid-to-gas phase transitions. *Science Robotics* **5**, eaaz4239 (2020), doi:10.1126/scirobotics.aaz4239.

9. Y. I. Kim, *et al.*, Nanotextured Soft Electrothermo-Pneumatic Actuator for Constructing Lightweight, Integrated, and Untethered Soft Robotics. *Soft Robotics* **9** (5), 960–969 (2022), doi:10.1089/soro.2020.0142.
10. R. Altmüller, R. Schwödiauer, R. Kaltseis, S. Bauer, I. M. Graz, Large area expansion of a soft dielectric membrane triggered by a liquid gaseous phase change. *Applied Physics A: Materials Science and Processing* **105** (1), 1–3 (2011), doi:10.1007/s00339-011-6311-1.
11. R. Niiyama, D. Rus, S. Kim, Pouch Motors: Printable/inflatable soft actuators for robotics, in *IEEE International Conference on Robotics and Automation (ICRA)* (2014), pp. 6332–6337, doi:10.1109/ICRA.2014.6907793.
12. S. Hirai, *et al.*, Micro elastic pouch motors: Elastically deformable and miniaturized soft actuators using liquid-to-gas phase change. *IEEE Robotics and Automation Letters* **6** (3), 5373–5380 (2021), doi:10.1109/LRA.2021.3075102.
13. R. Uramune, *et al.*, HaPouch: A miniaturized, soft, and wearable haptic display device using a Liquid-to-Gas phase change actuator. *IEEE Access* **10**, 16830–16842 (2022), doi:10.1109/ACCESS.2022.3149046.
14. K. Narumi, *et al.*, Liquid Pouch Motors: Printable Planar Actuators Driven by Liquid-to-Gas Phase Change for Shape-Changing Interfaces. *IEEE Robotics and Automation Letters* **5** (3), 3915–3922 (2020), doi:10.1109/LRA.2020.2983681.
15. M. Sogabe, F. C. Uetrecht, T. Kanno, T. Miyazaki, K. Kawashima, A quick response soft actuator by miniaturized liquid-to-gas phase change mechanism with environmental thermal source. *Sensors and Actuators A: Physical* **361**, 114587 (2023), doi:https://doi.org/10.1016/j.sna.2023.114587.
16. W. Wagner, A. Pruß, The IAPWS Formulation 1995 for the Thermodynamic Properties of Ordinary Water Substance for General and Scientific Use. *Journal of Physical and Chemical Reference Data* **31** (2), 387–535 (2002), doi:10.1063/1.1461829.
17. S. M. Mirvakili, A. Leroy, D. Sim, E. N. Wang, Solar-Driven Soft Robots. *Advanced Science* **8**, 2004235 (2021), doi:10.1002/advs.202004235.

18. Y. Shao, *et al.*, 4D printing Light-Driven soft actuators based on Liquid-Vapor phase transition composites with inherent sensing capability. *Chemical Engineering Journal* **454**, 140271 (2023), doi:10.1016/j.cej.2022.140271.
19. J. Lin, *et al.*, Laser-induced porous graphene films from commercial polymers. *Nature Communications* **5**, 5714 (2014), doi:10.1038/ncomms6714.
20. Y. Chyan, *et al.*, Laser-Induced Graphene by Multiple Lasing: Toward Electronics on Cloth, Paper, and Food. *ACS Nano* **12** (3), 2176–2183 (2018), doi:10.1021/acsnano.7b08539.
21. A. Dallinger, P. Kindlhofer, F. Greco, A. M. Coclite, Multiresponsive Soft Actuators Based on a Thermoresponsive Hydrogel and Embedded Laser-Induced Graphene. *ACS Applied Polymer Materials* **3** (4), 1809–1818 (2021), doi:10.1021/acsapm.0c01385.
22. Y. Xu, Q. Fei, M. Page, *et al.*, Laser-induced graphene for bioelectronics and soft actuators. *Nano Research* **14**, 3033–3050 (2021), doi:10.1007/s12274-021-3441-9.
23. Y. Cengel, *Introduction To Thermodynamics and Heat Transfer*, second ed. (2008).
24. Q. Mu, S. Feng, G. Diao, Thermal conductivity of silicone rubber filled with ZnO. *Polymer Composites* **28**, 125–130 (2007), doi:10.1002/pc.20215.
25. A. F. Mills, *Heat Transfer* (Prentice-Hall, New Jersey), second ed. (1999).
26. A. Miriyev, G. Caires, H. Lipson, Functional properties of silicone/ethanol soft-actuator composites. *Materials and Design* **145**, 232–242 (2018), doi:10.1016/j.matdes.2018.02.076.
27. Smooth-On, Inc., Ecoflex 00-45 Near Clear (2024), <https://www.smooth-on.com/sds/10000816-10000839.pdf> (accessed January 18th, 2025).
28. C. Kandilli, K. Ulgen, Solar Illumination and Estimating Daylight Availability of Global Solar Irradiance. *Energy Sources, Part A: Recovery, Utilization, and Environmental Effects* **30** (12), 1127–1140 (2008), doi:10.1080/15567030601100688.
29. J. Viitanen, J. Lehtovaara, E. Tetri, L. Halonen, User Preferences in Office Lighting: A Case Study Comparing LED and T5 Lighting. *LEUKOS* **9** (4), 261–290 (2013), doi:10.1582/LEUKOS.2013.09.04.003.

Acknowledgement

This work was supported by JSPS KAKENHI Grant Number JP24K21213. I sincerely thank my cats, whose eyes served as a visual reference for the demonstration of the tapetum lucidum structure and whose presence brought inspiration and support throughout the research process.

Author declaration

No competing financial interests exist.

CRedit

Maina Sogabe: Conceptualization, Data curation, Investigation, Formal analysis, Methodology, Supervision, Visualization, Writing – original draft, Writing – review & editing

Youhyun Kim: Data curation, Methodology, Formal analysis, Resources, Writing – original draft, Writing – review & editing

Kenji Kawahima: Funding acquisition, Investigation, Formal analysis, Project administration, Supervision, Writing – original draft, Writing – review & editing

8 Supplementary Material

1. Supplementary Figure S1: Changes in temperature increase at liquid-interface surfaces with directional light irradiation: Thermographic analysis of temperature increase at liquid-contact interfaces comparing two irradiation patterns on LIG-transferred silicone sheets: (A) irradiation from silicone side to LIG side (proposed method) and (B) irradiation from LIG side to silicone side, with (C) showing reference values for silicone-only sheets. The proposed method with irradiation from the silicone side demonstrated higher initial temperature change rate (first 5 seconds after light exposure).
2. Supplementary Movie S1: The actuator's bending under light irradiation and its bending release upon turning off the light.

3. Supplementary Movie S2 :Demonstration of a bio-inspired (Venus flytrap) robot utilizing the proposed actuator in a biomimetic movement driven by light.